International Journal of Multiphase Flow 36 (2010) 870–881

Contents lists available at ScienceDirect

International Journal of Multiphase Flow

journal homepage: www.elsevier.com/locate/ijmulflow

An experimental and theoretical study of particle deposition due to thermophoresis and turbulence in an annular flow

D.P. Healy [a], J.B. Young [b,*]

[a] Ove Arup Ltd., 13 Fitzroy Street, London W1T 4BQ, UK
[b] Hopkinson Laboratory, Cambridge University Engineering Department, Trumpington Street, Cambridge CB2 1PZ, UK

ARTICLE INFO

Article history:
Received 18 May 2010
Received in revised form 27 July 2010
Accepted 28 July 2010
Available online 10 August 2010

Keywords:
Two-phase flow
Thermophoresis
Particle deposition
Turbulent pipe-flow
Annular-flow

ABSTRACT

The paper describes an experimental and theoretical study of the deposition of small particles from a turbulent annular-flow with cross-stream temperature variation, focusing on the effects of thermophoresis. Various expressions for the thermophoretic force on a spherical particle are critically discussed. The well-known composite formula of Talbot et al. (1980) does not include the 'second mechanism of thermophoresis' and it is concluded that the more recent theoretical approach of Beresnev and Chernyak (1995) is probably more reliable. New experimental measurements of particle deposition from a turbulent flow with cross-stream temperature gradients are then presented. The measurement technique is similar to the method of Liu and Agarwal (1974) but in the test section the aerosol flows vertically downwards in an annular gap between two concentric pipes. By heating the outer pipe and cooling the inner it is possible to establish a substantial, near-constant temperature difference between the two walls and hence a thermophoretic force which varies only with radius. Numerical calculations provide a comparison of theory with experiment. The theory is based on the turbulent deposition models of Young and Leeming (1997) and Slater et al. (2003) modified to include thermophoresis and the annular geometry. The theory of Beresnev and Chernyak gives good agreement with the experimental measurements.

1. Introduction

Small particles suspended in a gas with a non-uniform temperature distribution experience a force which usually acts in the opposite direction to the temperature gradient. The phenomenon is known as thermophoresis and finds application in several areas of engineering. The authors are particularly interested in particle deposition on the turbine blades of coal-fired gas turbines. Modern gas turbines for power generation have turbine inlet temperatures of about 1500 °C but material considerations require that the blade temperature does not exceed about 850 °C. This results in high temperature gradients near the blade surfaces and small coal ash particles, entrained into the turbulent boundary layers, experience a thermophoretic force which enhances deposition rates.

Most experimental and theoretical studies of particle deposition have been carried out in fully-developed turbulent pipe-flow as exemplified by the frequently cited work of Liu and Agarwal (1974). The attractiveness of such experiments is that the relatively simple gas-particle flowfield features many of the characteristics found in more complex situations. To date, most experiments have involved isothermal flows and the focus has been on the effects of turbulence. Recently, however, thermophoresis has received more attention and experiments have been carried out in turbulent pipe-flow with cross-stream temperature gradients by Leeming (1995) and Romay et al. (1998). Unfortunately, however, it has proved difficult to establish a substantial radial temperature difference which does not vary along the pipe and this has compromised the usefulness and accuracy of the measurements. The present paper describes a new experimental arrangement involving flow in the annular region between two concentric pipes which is designed to overcome this inadequacy.

Quite apart from problems involving the interaction of turbulence with thermophoresis, the thermophoretic force experienced by a spherical particle under laminar flow conditions is still an issue. There have been many studies (see reviews by Talbot et al. (1980) and Bakanov (1991)) but no definitive theory spanning the whole range of Knudsen numbers has emerged. A composite expression suggested by Talbot et al. (1980) has become widely accepted and this will be critically examined in the light of the new experimental results.

The scheme of the paper is as follows. Section 2 examines various expressions for the thermophoretic force and the validatory experimental measurements. Section 3 then highlights the inadequacies of the existing data for deposition in turbulent pipe-flow and Section 4 describes the new experimental measurements. The deposition theory of Young and Leeming (1997) has been mod-

* Corresponding author. Tel.: +44 (0) 1223330263.
E-mail addresses: david.healy@arup.com (D.P. Healy), jby@eng.cam.ac.uk (J.B. Young).

0301-9322/$ - see front matter © 2010 Elsevier Ltd. All rights reserved.
doi:10.1016/j.ijmultiphaseflow.2010.07.006

ified for turbulent annular-flow with thermophoresis and forms the basis for the computational scheme described in Section 5. Finally, in Section 6, the new measurements are compared with calculations using various expressions for the thermophoretic force.

2. Theoretical expressions for the thermophoretic force

In non-dimensional form, the thermophoretic force $\mathbf{F}_T$ acting on a spherical particle of radius r_p can be written,

$$\frac{\mathbf{F}_T \rho_g}{\mu_g^2} = \Phi \frac{r_p \nabla T_g}{T_g} \tag{1}$$

where ρ_g, T_g and μ_g are the density, temperature and dynamic viscosity which the gas would have at the centre of the particle were the particle absent, ∇T_g is the temperature gradient in the absence of the particle and $\Phi = \Phi(Kn, \Lambda)$ is a function of the particle Knudsen number Kn and the thermal conductivity ratio Λ. The Knudsen number is defined by,

$$Kn = \frac{l_g}{r_p} \tag{2}$$

where l_g is the molecular mean free path and is obtained from the kinetic theory expression,

$$l_g = \mu_g \sqrt{\frac{\pi}{2 p_g \rho_g}} \tag{3}$$

where p_g is the gas pressure. The thermal conductivity ratio Λ is defined by,

$$\Lambda = \frac{k_p}{k_g} \tag{4}$$

where k_p is the particle thermal conductivity and k_g is the translational contribution to the gas thermal conductivity given by,

$$k_g = \frac{15}{4} \mu_g R_g \tag{5}$$

where R_g is the gas constant per unit mass.

In this paper Eqs. (3) and (5) are used to define l_g and k_g and provide the means for calculating the parameters Kn and Λ through Eqs. (2) and (4). It should be noted, however, that l_g and k_g are often defined with different coefficients (but the same form) and when comparing the results of theoretical calculations with experimental data or other theories it is most important to apply the necessary conversion factors so that the comparison is made on a common basis.

2.1. The theories of Waldmann, Epstein, Brock and Talbot et al.

Despite a large amount of theoretical work, there is still considerable uncertainty about the form of the function Φ defined by Eq. (1). This is particularly so in the slip-flow and transition regimes where $\mathbf{F}_T$ is strongly influenced by Λ. The various theoretical approaches for calculating Φ are now examined.

For the free-molecule regime ($Kn \gg 1$), Waldmann (1959) used kinetic theory to derive an expression that is still considered to be very reliable. His result for Φ is independent of Λ and is given in Table 1. The fact that Φ is a negative quantity implies that the thermophoretic force acts in the opposite direction to the temperature gradient.

Thermophoresis at low Knudsen numbers has proved more difficult to model. Epstein (1929) attempted to derive an equation for the slip-flow regime and he identified the importance of Λ at low Kn (see Table 1). However, when Brock (1962) reassessed the theory, he found that Epstein had used an incorrect slip-flow boundary condition and (less importantly) had neglected the convective terms in the energy equation. Correcting the analysis, he arrived at the more complex expression shown in Table 1 which reduces to Epstein's result as $Kn \to 0$.

Table 1
Theoretical expressions for the function Φ. See the text for details of the values of the constants in the various expressions.

Author and range of validity	$\Phi(Kn, \Lambda)$
Epstein (1929) $Kn \to 0$	$\frac{-12\pi K_{tc}}{(2+\Lambda)}$
Waldmann (1959) $Kn \to \infty$	$\frac{-2\pi}{Kn}$
Brock (1962) Talbot et al. (1980), All Kn	$\frac{-12\pi K_{tc}(1+C_e \Lambda Kn)}{(1+3C_m Kn)(2+\Lambda+2C_e \Lambda Kn)}$
Yamamoto and Ishihara (1988) All Kn	$\frac{-6\pi^{3/2}}{Kn}\left[\frac{A_w H_0 - A_0 (H_w + 2.5 \Lambda Kn)}{(H_w + 2.5 \Lambda Kn)}\right]$
Beresnev and Chernyak (1995) All Kn	$\frac{-2\pi}{Kn}\left[\frac{f_{11} + \Lambda f_{21}}{f_{31} + (1 + 2.5 \Lambda Kn) f_{41}}\right]$

As can be seen from Brock's expression, the theory of thermophoresis requires the values of three coefficients: the thermal creep coefficient K_{tc}, the velocity slip coefficient C_m and the temperature jump coefficient C_e. Both Epstein and Brock used Maxwell's value of $K_{tc} = 0.75$ for the thermal creep coefficient but more accurate solutions of the Boltzmann equation (see Beresnev and Chernyak, 1995) suggest that a value of around 1.125 is more appropriate.

The velocity slip and temperature jump coefficients C_m and C_e depend on the momentum and energy accommodation coefficients α_m and α_e according to,

$$C_m = \left(\frac{2 - \alpha_m}{\alpha_m}\right) A_m, \quad C_e = \left(\frac{2 - \alpha_e}{\alpha_e}\right) A_e \tag{6}$$

where A_m and A_e are constants. Simple kinetic theory approximations for a monatomic gas give $A_m = 1.0$ and $A_e = 15/8 = 1.875$ and these were the values used by Brock (1962). However, more recent work (see Beresnev and Chernyak, 1995) suggest that $A_m \cong 1.137$ and $A_e \cong 2.178$ are more appropriate values. The accommodation coefficients describe the interaction of the incident gas molecules with the particle surface and for practical calculations it is usually assumed that $\alpha_m = \alpha_e = 1$ as the true values are seldom known.

Brock's result was only intended to model the continuum and slip-flow regimes but Talbot et al. (1980) noticed that by slightly adjusting the values of K_{tc} and C_m the equation gave a good approximation to the Waldmann free-molecule expression for $Kn \to \infty$ (the expression is given exactly if $K_{tc} = C_m$). This interpolation prescription has been widely-used for practical calculations ever since, particularly as the values $K_{tc} = 1.17$, $A_m = 1.14$ and $A_e = 2.18$ suggested by Talbot et al. are close to the currently accepted values cited above. Fig. 1 shows how Φ varies with Kn for several values of Λ according to this prescription.

2.2. Theories for arbitrary Knudsen number

It is evident from Fig. 1 that Epstein's expression predicts large differences in Φ for low and high values of Λ in the continuum limit, $Kn \to 0$. The problem comes in linking this result through the transition regime with Waldmann's free-molecule expression because the Talbot et al. prescription is an interpolation formula and is not based on physical modelling.

Analytical theories of transition regime thermophoresis involve enormous difficulties because it is necessary to solve the Boltzmann equation in the vicinity of the particle with the correct far-field and particle surface boundary conditions. At the time of writing this has not yet been achieved although a number of authors have published solutions of model Boltzmann equations with simplified collision integral terms. Detailed examination shows that essentially all of this work is embodied in the solutions of Yamamoto and Ishihara

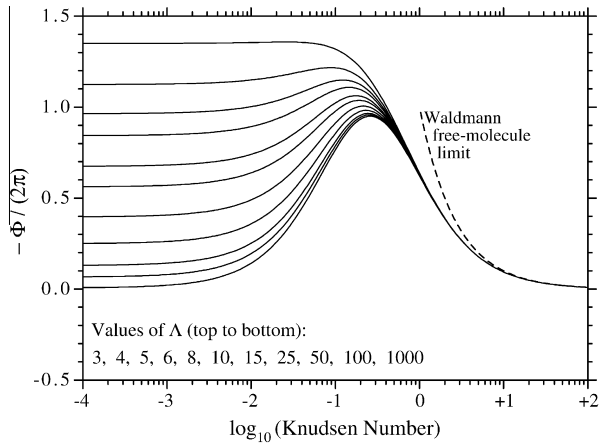

Fig. 1. Curves of $-\Phi/(2\pi)$ plotted against $\log_{10}(Kn)$ for various values of Λ using the interpolation formula of Talbot et al. (1980) with $\alpha_m = \alpha_e = 1$. All curves asymptote to Epstein's continuum limits as $Kn \to 0$.

(1988) and Beresnev and Chernyak (1995). The former used the original BGK equation as their starting point and the latter used the so-called S-model, a generalisation of the BGK equation devised by Shakhov (1968) which yields 13 correct moments of the velocity distribution function and should therefore provide a better approximation to the Boltzmann equation. In particular, the S-model gives the correct Prandtl number of 2/3 for a monatomic gas while the original BGK equation gives an incorrect value of unity.

Expressions for calculating Φ according to Yamamoto and Ishihara and Beresnev and Chernyak are given in Table 1. The constants in these expressions were calculated numerically by the authors and are given in tabular form for discrete values of the Knudsen number in the original papers. Fig. 2 shows how Φ varies with Kn for selected values of Λ and emphasises the very large differences between the solutions based on these two models and the Talbot et al. interpolation prescription.

A major feature of the Yamamoto and Ishihara calculations is the existence of a region of 'negative' or 'reversed' thermophoresis at low Kn and high Λ. This phenomenon does not appear at all in the Talbot et al. interpolations. It is just present, although with greatly diminished magnitude, in the Beresnev and Chernyak calculations, but only at very high values of Λ (which are not shown in Fig. 2).

Reversed thermophoresis was first predicted theoretically by Dwyer (1967) and was explained in physical terms by Sone (1972). Briefly, when $\Lambda \gg 1$ the temperature of the particle is almost uniform and Maxwell's thermal creep flow is negligible. Then, the thermal stress slip-flow, a higher-order effect known as the 'second mechanism of thermophoresis', determines the flowfield. With respect to the particle, the gas flows from the hotter to the colder region and the particle is subjected to a force in the opposite direction. Reversed thermophoresis has never been demonstrated unambiguously in an experiment.

2.3. Experimental data

It is very difficult to obtain accurate experimental measurements of the thermophoretic force, particularly at low Kn and high Λ (Bakanov, 1991). The most reliable data have been obtained using a Millikan cell apparatus, modified with hot and cold parallel plates to establish the temperature gradient. Fig. 3 shows a comparison of selected data from the experiments of Schmitt (1959) and Jacobsen and Brock (1965) with the theoretical predictions of Beresnev and Chernyak. The experimental points were obtained by hand measurements from the original graphs followed by data processing to obtain the values of Φ. The agreement with the Beresnev and Chernyak theory is very good and this is generally true of the older data.

Fig. 4 shows selected processed data from the extensive experimental study by Li and Davis (1995a,b). The Beresnev and Chernyak theory tends to underpredict the data and the agreement is not as good as in Fig. 3. Although this trend is typical of the more recent data (which often displays considerable scatter and some inconsistency), the Beresnev and Chernyak theory always outperforms that of Yamamoto and Ishihara and is usually better than that of Talbot et al. It is therefore concluded that, with the present state of knowledge, the Beresnev and Chernyak theory is currently the best available method for predicting the thermophoretic force on a spherical particle at arbitrary Knudsen number and thermal conductivity ratio.

Finally, it should be noted that all theoretical work to date has been concerned with predicting the thermophoretic force in a steady temperature gradient. The effects of an unsteady temperature field, either deterministic or random (i.e., turbulent in origin), are quite unknown.

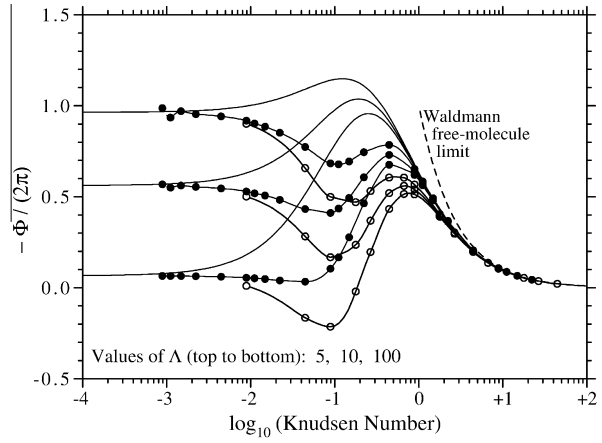

Fig. 2. Curves of $-\Phi/(2\pi)$ plotted against $\log_{10}(Kn)$ for selected values of Λ. The white circles are from Yamamoto and Ishihara (1988), the black circles are from Beresnev and Chernyak (1995), and the solid lines are the interpolation of Talbot et al. (1980), all for $\alpha_m = \alpha_e = 1$.

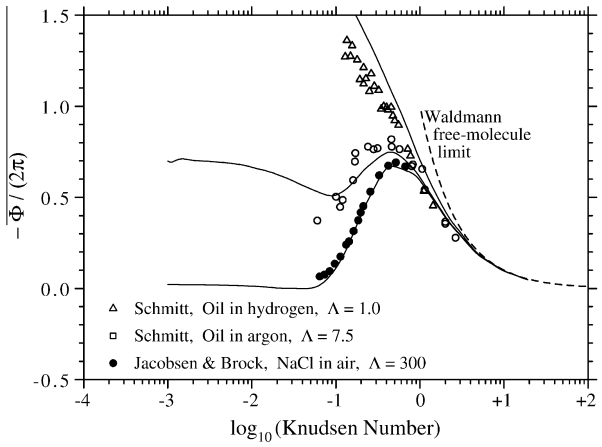

Fig. 3. Comparison of the data of Schmitt (1959) for oil droplets in hydrogen and argon, and Jacobsen and Brock (1965) for NaCl spheres in air with the theoretical predictions of Beresnev and Chernyak (1995) for $\Lambda = 1.0$, 7.5 and 300, all for $\alpha_m = \alpha_e = 1$.

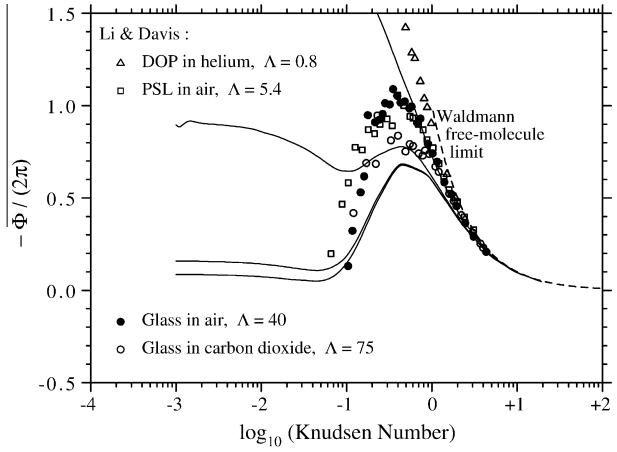

Fig. 4. Comparison of the data of Li and Davis (1995a, 1995b) for dioctyl phthalate droplets in helium, polystyrene latex spheres in air, glass spheres in air and glass spheres in CO_2 with the theoretical predictions of Beresnev and Chernyak (1995) for (top to bottom) Λ = 0.8, 5.4, 40 and 75, all for $\alpha_m = \alpha_e = 1$.

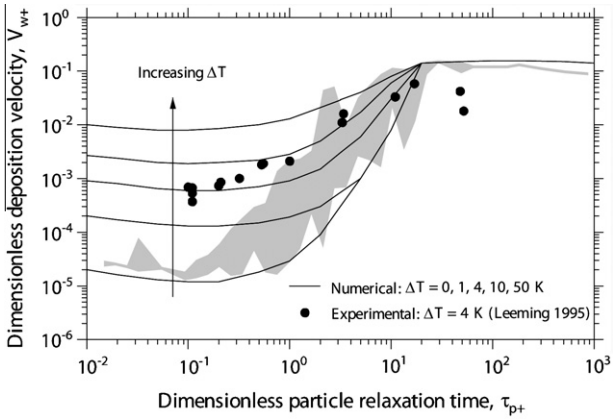

Fig. 5. Deposition in a turbulent pipe-flow with a cross-stream temperature difference. The shaded area represents the *isothermal* experimental data collected by Young and Leeming (1997): Friedlander and Johnstone, Schwendiman and Postma, Wells and Chamberlain, Sehmel and Liu and Agarwal. The *non-isothermal* numerical calculations are from Slater et al. (2003).

3. Turbulent pipe-flow experiments with a cross-stream temperature gradient

We now consider the flow of a dilute mixture of gas and monodispersed, spherical particles in a vertical pipe of diameter D. The particle mass density ρ_p is defined as the mass of particles per unit volume and the flow-averaged value $\rho_{p,m}$ is defined such that the mass flowrate of particles is given by $\rho_{p,m} U_m \pi D^2/4$ where U_m is the mean flow velocity. Experimental measurements of deposition rate in isothermal, fully-developed pipe-flow are usually reported (Liu and Agarwal, 1974) by plotting the dimensionless deposition velocity at the wall V_{w+} against the dimensionless particle relaxation time τ_{p+}. V_{w+} is defined by,

$$V_{w+} = \frac{J_w}{u_* \rho_{p,m}} \tag{7}$$

where J_w is the mass flux of particles to the wall (i.e., per unit wall area) and u_* is the friction velocity. τ_{p+} is defined by,

$$\tau_{p+} = \frac{\rho_{mat} \rho_g d_p^2 u_*^2}{18 \mu_g^2} \tag{8}$$

where ρ_{mat} is the particle material density and d_p is the particle diameter.

Several studies of thermophoretic particle deposition in laminar pipe-flow have been carried out (e.g., Montassier et al., 1991) and there have also been two investigations in turbulent pipe-flow by Leeming (1995) and Romay et al. (1998). Romay et al. used sodium chloride and polystyrene latex particles in a vertical turbulent pipe-flow. The particle-laden flow was heated to between 25 °C and 137 °C at pipe entry, while the water-cooled wall was maintained at 20 °C. Condensation nucleus counters (CNCs) upstream and downstream of the pipe were used to measure the deposition efficiency η_{dep}. In order to decouple the thermophoretic component of η_{dep} from the overall value it was assumed that thermophoresis did not interact with any other deposition mechanism. The experimental results were then found to be 1.4–2.0 times greater than the predictions using the equation of Talbot et al.

The problem with this approach can be seen by considering the relationship between η_{dep} and the average value of dimensionless deposition velocity $\bar{V}_{w+}$,

$$\bar{V}_{w+} = -\frac{U_m D}{4 u_* L} \ln(1 - \eta_{dep}) \tag{9}$$

where L is the length of the pipe. The derivation of Eq. (9) can be found in Sehmel (1968). Whereas Liu and Agarwal determined V_{w+} by cutting the pipe into sections, finding V_{w+} for each section and then taking an average, Romay et al. used the CNCs to determine η_{dep} and hence a single value of $\bar{V}_{w+}$. For fully-developed isothermal flow this may be acceptable but in the experiments of Romay et al. the flow cooled along the pipe thus giving rise to a variable cross-stream temperature difference. The conversion of η_{dep} to $\bar{V}_{w+}$ for the entire pipe is then problematic as V_{w+} varies quite strongly in the axial direction.

The experiments of Leeming (1995) avoided this problem. Leeming performed experiments with particles of oleic acid and uranine in a turbulent pipe-flow similar to that of Liu and Agarwal. The particle-laden flow was heated and flowed downwards through a vertical pipe with water-cooled walls. The mass deposited on the pipe wall was determined by cutting the pipe into sections and using fluorescence spectrometry. The flowrate of cooling water was carefully chosen to give a constant heat flux through the wall resulting in a constant temperature difference. Unfortunately, it was found that when the flow had travelled sufficiently far along the pipe for the temperature profile to be fully-developed, the cross-stream temperature difference was only about 4 °C. Hence, although axial variations were small, only a single temperature difference of 4 °C could be established. Fig. 5 shows the data from these experiments compared with the numerical calculations of Slater et al. (2003) using the expression of Talbot et al. for the thermophoretic force. Although sparse, the data are in fairly good agreement with the calculations except for two points at high values of τ_{p+}.

4. New experiments in turbulent annular-flow

In order to overcome the deficiencies of the pipe-flow experiments, a new experimental configuration was designed which involved the particle-laden air flowing in the annular region between two concentric pipes of different diameters. This will be referred to as turbulent annular-flow.[1] The inner wall was cooled and the outer wall heated so that both wall temperatures remained fairly constant along the length of the test section. It was then possible to achieve a fully-developed temperature field with large

[1] This is definitely not to be confused with annular gas–liquid flow where the liquid moves as a film on the pipe wall and the gas flows in the core region.

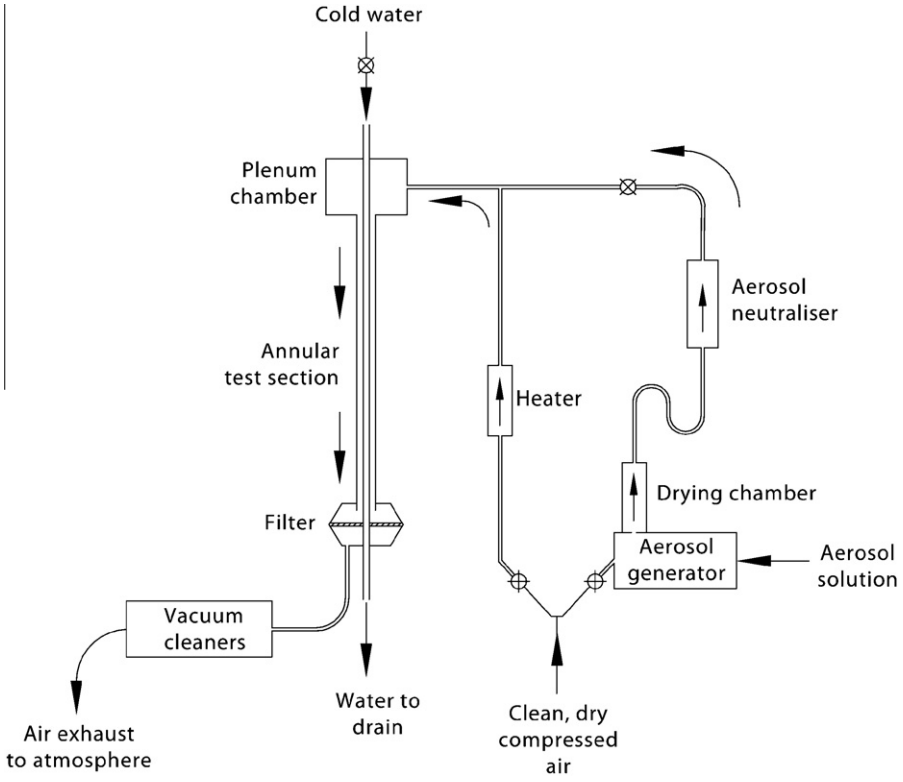

Fig. 6. A schematic diagram of the experimental equipment.

radial temperature differences and only minor axial variations in gas properties and thermophoretic force.

4.1. The experimental equipment

The general experimental setup and procedure are similar to those of Liu and Agarwal (1974) and Leeming (1995). Full details are given by Healy (2003) and only a brief description focusing on the annular test section will be given here. A schematic diagram of the equipment is shown in Fig. 6.

A TSI model 3450 vibrating orifice aerosol generator was used to generate particles that consisted of a solid core of uranine (used as a fluorescent tracer) surrounded by a liquid coating of oleic acid (to promote adhesion when deposition occurred). A supply of clean dry compressed air entered the aerosol generator and left it carrying an electrically charged cloud of aerosol particles which was neutralised by flowing past a 10 mCi krypton-85 radioactive source. The particle-laden flow was then mixed with a secondary air flow because the required flowrate was higher than the rated output of the aerosol generator (100 lpm). The secondary flow passed through a 1600 W threaded inline heater in order to raise the temperature of the aerosol flow before entry to the annular test section. This reduced the length of annulus required to attain a fully-developed temperature field. Before entering the test section, the flow passed through a plenum chamber which ensured good mixing and prevented swirl in the annulus. The existence of even a small swirl component can have a major effect on deposition measurements.

From the plenum chamber, the flow entered the annular test section which consisted of a 15 mm outside diameter stainless steel tube placed concentrically in a 23 mm inside diameter brass pipe. The brass pipe was 2.4 m in length and extended from the bottom of the plenum chamber to the top of a filter assembly. The stainless steel tube was longer and passed through the top of the plenum chamber and the bottom of the filter assembly. Cold water was directed downwards through the tube at a flow rate of 30 lpm which was sufficient to maintain a constant wall temperature. The aerosol flow passed from the plenum chamber, vertically downwards between the steel tube and brass pipe, and into the filter assembly. This consisted of a 110 mm diameter Whatman glass microfibre (GF/A) filter with either 1.6 or 1.0 μm retention to capture any particles which remained suspended in the flow. An 800 W (5 m × 25 mm) heating tape was wrapped around the outside of the brass pipe and a controller was used to adjust the power to the tape thus maintaining the pipe at a constant temperature. The plenum chamber, filter assembly, heating tape and brass tube were lagged to prevent heat loss. Both the tube and the pipe were earthed to remove any electrical charge that might have affected deposition.

As a further precaution against swirl, a 12-finned 25 mm long flow straightener was fitted at the entrance to the annular test section. A similar device was attached to the lower end of the annulus and together they also served the purposes of locating the inner tube concentrically within the outer pipe and preventing the removal of deposited particles when the inner tube was removed from the outer for washing. A novel technique was developed for washing each wall of the annulus in sections and the washings were analysed using a LS-30 Perkin–Elmer luminescence spectrometer. The first and last sections of the annulus were not used for measurement of deposition velocity because of entrance and exit effects, and also because the flow straighteners would tend to distort the measurements in these areas. Eq. (9) was used to demonstrate that such effects did not persist by plotting the theoretical deposition efficiency (for the measured average deposition velocity) along the entire length of the pipe and comparing it with the measured values. These procedures are described in detail by Healy (2003). It is worth noting that this method of obtaining the variation of deposition velocity along the test section is extremely time-consuming and labour-intensive. Each single point on a graph of V_{w+} versus τ_{p+} (such as in Fig. 9 below) required at least two

days full-time work. Allowing for one or two repetitions to check consistency increased the cost to around one graphical point per week!

4.2. Isothermal experiments and measurements

A set of isothermal experiments was first carried out to provide a datum and a link to other pipe-flow experiments. This involved taking data without the use of the inline heater, heating tape, or cooling water. For the radius ratio employed (23/15 = 1.53), Chung et al. (2002) found that the turbulence quantities close to the inner wall of an annulus are similar to those of a plane 2D channel-flow, and the outer wall profiles are similar to those of a pipe-flow. Since deposition in 2D channel-flow and pipe-flow are thought to be similar, V_{w+} on each wall of the annulus was expected to be similar to that of a turbulent pipe-flow.

There were certain limitations on the annulus dimensions. Thus, a relatively large gap was required to ensure that deviations from concentricity were small and that the inner pipe could be removed from the outer without the unwanted removal of deposited particles. The hydraulic diameter chosen to fulfil these requirements ($D_h = 23 - 15 = 8$ mm) was similar to the pipe diameters used by Liu and Agarwal and Leeming (12.7 and 10 mm) but the flow cross-sectional area was much greater. Hence, in order to achieve the Reynolds numbers used by these authors (50,000 and 20,000), it would have been necessary to supply the compressed air at pressures far in excess of the maximum allowed by the aerosol generator. Although two vacuum motors were arranged in parallel downstream of the filter assembly to increase the air flowrate, the maximum Reynolds number possible (based on D_h) was only about 6000.

Eq. (8) shows that τ_{p+} can be increased either by increasing d_p or by increasing u_* through an increase in the Reynolds number. Liu and Agarwal and Leeming achieved large values of τ_{p+} by increasing the Reynolds number but, as this option was not available for the annular-flow experiments, τ_{p+} was controlled by varying d_p. Because of the difficulty in measuring out small quantities of uranine and oleic acid it was difficult to produce an aerosol with particles smaller than 1 μm in diameter, while particles larger than 25 μm resulted in persistent clogging of the small orifice disks. The range of τ_{p+} was accordingly limited to about 0.1–100. More importantly, however, the transition from the plenum chamber to the annulus proved to be very effective at 'capturing' large particles so that the maximum achievable test section value of τ_{p+} was no more than 8 (see Healy (2003), for further details).

Fig. 7 shows the results of the isothermal experiments with V_{w+} plotted for each wall separately. For comparison, other isothermal *pipe-flow* measurements have been included (represented by the shaded area), together with the experiments of Wells and Chamberlain (1967) which were carried out with an *annular-flow* (although only inner wall deposition velocities were measured). Fig. 7 shows that the outer wall deposition velocities are slightly larger than those on the inner wall but that both are contained within the envelope of the pipe-flow results and that the agreement with the Wells and Chamberlain data is good. For $\tau_{p+} > 8$, V_{w+} does not behave as expected due to the plenum chamber capture problem.

4.3. Thermophoresis experiments and measurements

For the thermophoresis experiments the outer wall was maintained at one of three nominal temperatures, $T_{ow} \cong 40$ °C, 85 °C or 140 °C. Uranine starts to soften at temperatures above 90 °C (Al-Azzawi and Owen, 1984) but this temperature was only exceeded very close to the hot wall for $T_{ow} \cong 140$ °C. The inner wall temperature T_{iw} remained almost constant along the length of the pipe at 12 °C for all tests.

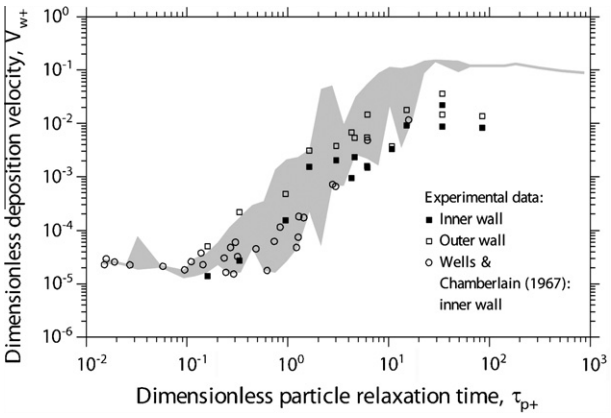

Fig. 7. Experimental results for *isothermal* turbulent annular-flow. The shaded area represents a compilation of experimental results for isothermal turbulent *pipe-flow*.

The electrical power to the heating tape was set by a controller which maintained the local temperature constant to within 2–4 °C. The outer wall temperature was measured by several thermocouples stationed along the pipe and the axial temperature profiles for the 140 °C tests are shown in Fig. 8. In the section, 60–160 cm used for the deposition measurements, T_{ow} increases by about 20 °C (and correspondingly less for the tests with lower wall temperature). The temperature difference across the annulus was therefore not quite constant but the variation was normally less than 15%. For the purposes of analysis, a single average outer wall temperature was ascribed to each experiment.

To put the experimental results in context, it should be noted that the thermal conductivities of uranine and oleic acid are 0.43 and 0.23 W m^{-1} K^{-1} respectively, so that $\Lambda = k_p/k_g = 11$–21. The Knudsen number varied from 0.015 to 0.136. These values place the experiments in the slip-flow regime with a moderate thermal conductivity ratio, see Fig. 2.

The results of the experiments for the three outer wall temperatures are shown in Fig. 9. Considering the series for $T_{ow} \cong 40$ °C, it can be seen that, for the four smallest values of τ_{p+}, the inner wall deposition velocities are almost identical and an order of magnitude greater than the isothermal values. The outer wall deposition velocities were too low to be measured. In this region ($\tau_{p+} < 0.5$) thermophoresis dominates over turbulent-Brownian diffusion

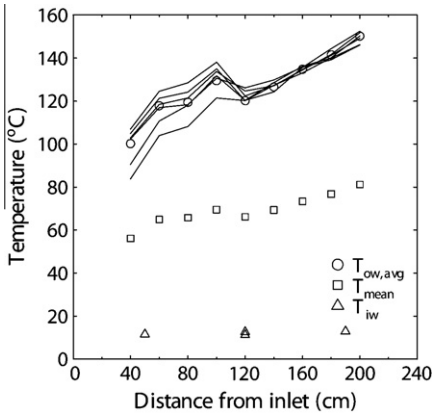

Fig. 8. Axial temperature profiles for $T_{ow} \cong 140$ °C, the largest outer wall temperature used in the experiments. The solid lines represent the outer wall profiles for each individual experiment and these have been averaged locally to give a $T_{ow,avg}$ profile. The T_{mean} profile is then the average of $T_{ow,avg}$ and T_{iw}.

(the mechanism responsible for deposition in the absence of a temperature gradient) and turbophoresis is unimportant (because with such low inertia the particles do not slip relative to the carrier-gas eddies). Thermophoresis drives particles towards the cold inner wall (enhancing deposition rates as shown in Fig. 9) and away from the hot outer wall (reducing deposition rates to zero if the thermophoretic effect is sufficiently strong).

In the range $0.5 < \tau_{p+} < 5.0$, both inner and outer wall deposition velocities increase, the latter very rapidly. In fact, the accuracy of the low outer wall values is probably not good because of the difficulty in measuring the small quantities of uranine deposited but the trend is clear. At $\tau_{p+} \cong 5.0$, both inner and outer wall deposition velocities are approximately equal to the isothermal value implying that particle inertia has increased to such an extent that deposition is dominated by turbophoresis and the contribution from thermophoresis is negligible. The Knudsen number at this point is about 0.02. At $\tau_{p+} = 8.0$ the validity of the data is doubtful because of the probability of aerosol depletion caused by deposition in the approach ducting and plenum chamber.

In the transition region $0.5 < \tau_{p+} < 5.0$ thermophoresis and turbophoresis are both important. Whether the two effects are simply superposed or whether there is a more complex interaction as speculated by Romay et al. (1998) is difficult to deduce from the measurements. However, taking a closer look at the experimental results in Fig. 10, it is noticeable that the data points for $T_{ow} \cong 40$ °C start to curve upwards at $\tau_{p+} \cong 0.5$, a level of particle inertia where turbophoresis would not normally make any significant contribution to deposition.

As can be seen in Figs. 9 and 10, the data sets for $T_{ow} \cong 85$ °C and 140 °C show similar behaviour. Taken together, the three sets of data confirm that, as expected, the inner wall deposition velocity increases with increase in T_{ow} although the relationship is not linear with temperature because the thermophoretic force is proportional to $\nabla T_g/T_g$ rather than ∇T_g. Finally, it should also be noted that the data (with the exception of the points at $\tau_{p+} = 8.0$) are very self-consistent and give confidence that the measurements have good accuracy.

5. The numerical calculation scheme

Predictions of particle deposition rates in fully-developed turbulent annular-flow were carried out using an extension of the approach of Young and Leeming (1997) with the averaging method of Slater et al. (2003).

The Eulerian solution scheme of Young and Leeming (1997) used non-particle-density-weighted averaging (referred to as Reynolds-averaging) of the particle conservation equations and was formulated specifically for the problem of deposition in a turbulent pipe-flow. Particular emphasis was placed on treating the equations in such a way that the different roles of diffusion (particle fluxes driven by particle-density gradients) and turbophoresis (particle fluxes driven by fluctuating particle-velocity gradients) were highlighted. All particle flows are compressible, however, and it is often advantageous to use particle-density-weighted averaging (referred to as Favre-averaging) of the particle equations because this reduces the number of turbulence correlations generated. This approach was adopted by Slater et al. (2003) for their calculations of more general two-dimensional gas-particle flows.

For a full description of the averaging procedure and modelling of the particle turbulence correlations the reader is referred to the papers by Young and Leeming and Slater et al. Details of the application of the methodology to deposition in a turbulent annular-flow, including the specification of the carrier-gas turbulence quantities can be found in Healy (2003). However, in order to make the present paper self-consistent and to assist the reader in interpreting the results of the analysis, a brief presentation of the governing equations is now given.

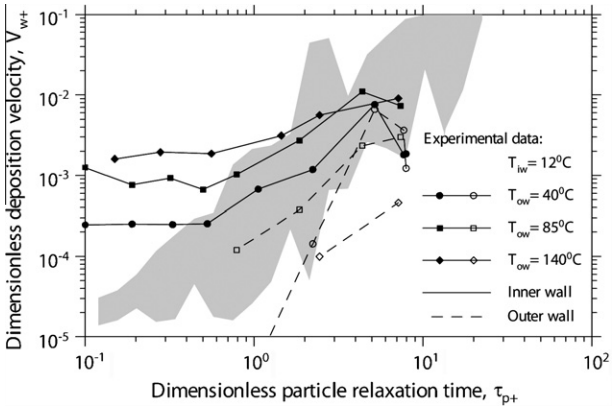

Fig. 9. Results for the thermophoresis experiments in turbulent annular-flow with three different outer wall temperatures. The shaded area represents the same data as in Fig. 7 although a different scale is used.

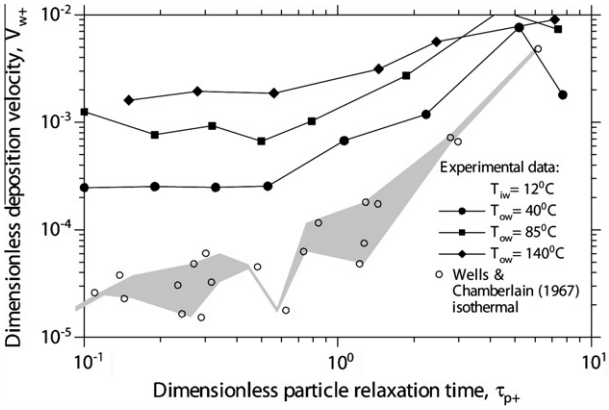

Fig. 10. Results for the thermophoresis experiments in turbulent annular-flow with three different outer wall temperatures – a closer examination of deposition velocities in the transitional region. The shaded area highlights the *isothermal* inner wall data of Wells and Chamberlain (1967).

5.1. The particle conservation equations and boundary conditions

Following Healy (2003), and making a number of simplifications for fully-developed axisymmetric flow, the Favre-averaged particle momentum equations in the radial and axial directions written in dimensionless form are,

$$\overline{\overline{W}_{p,r+}}\frac{\partial \overline{\overline{W}_{p,r+}}}{\partial r_+} = -\frac{\partial \overline{(\overline{v'_{p,r+}}\, \overline{v'_{p,r+}})}}{\partial r_+} - \frac{\phi_D \overline{\overline{W}_{p,r+}}}{\tau_{p+}} + \overline{\overline{F}_{L,r+}} + \overline{\overline{F}_{T,r+}} \qquad (10a)$$

$$\overline{\overline{W}_{p,r+}}\frac{\partial \overline{\overline{W}_{p,z+}}}{\partial r_+} = \frac{\partial}{\partial r_+}\left(\nu_{gt+}\frac{\partial \overline{\overline{W}_{p,z+}}}{\partial r_+}\right) + \frac{\phi_D(\overline{U_{g,z+}} - \overline{\overline{W}_{p,r+}})}{\tau_{p+}} + g_+ \qquad (10b)$$

where a double overbar denotes a Favre-averaged quantity and a single overbar a Reynolds-averaged quantity. In Eqs. (10) r is the radial distance measured from the axis, z is the axial distance, $\mathbf{U}_g$ is the carrier-gas velocity, $\mathbf{W}_p$ is the particle convective velocity, $v'_{p,r}$ is the radial component of the particle (not gas) fluctuating-velocity, $\mathbf{F}$ is force per unit mass with the subscripts L and T referring to lift and thermophoresis, ϕ_D is a function of the particle slip Reynolds number and accounts for non-Stokesian drag, ν_{gt} is the carrier-gas turbulent viscosity and g is the gravitational acceleration.

All quantities are non-dimensionalised using wall variables: $r_+ = r u_*/\nu_g$, $g_+ = g\nu_g/u_*^3$, $v_{gt+} = \nu_{gt}/\nu_g$, $\mathbf{F}_+ = \mathbf{F}\nu_g/u_*^3$, $\mathbf{U}_{g+} = \mathbf{U}_g/u_*$, $\mathbf{W}_{p+} = \mathbf{W}_p/u_*$ and $v'_{p,r+} = v'_{p,r}/u_*$.

The definition of the particle convective velocity is most important for the method of analysis. Very briefly, the total particle mass flux is decomposed into the sum of two fluxes, one convective and one diffusive. The particle convective velocity is then obtained by dividing the convective mass flux by the local particle mass density ρ_p (mass of particles per unit volume). If the convective velocity is defined in this way, it turns out that ρ_p can be eliminated completely from the momentum equations, as in Eqs. (10). This is extremely convenient both for the purposes of physical interpretation and also for numerical solution. Full details of this important procedure can be found in Slater et al. (2003).

Young and Leeming (1997) defined a dimensionless Reynolds-averaged particle density $\bar{\psi}$ by the equation,

$$\bar{\psi}(r) = \frac{\bar{\rho}_p(r,z)}{\bar{\rho}_{p,m}(z)} \tag{11}$$

where $\bar{\rho}_{p,m}(z)$ is the mean value across the annulus (as defined in Section 3) of the Reynolds-averaged particle mass density $\bar{\rho}_p$. This definition was designed to remove the dependency of particle density on axial position. The Favre-averaged particle mass conservation equation in dimensionless form then becomes,

$$\frac{1}{r_+}\frac{d}{dr_+}\left(r_+\bar{\psi}\overline{\overline{W_{p,r+}}}\right) - K_+\bar{\psi}\overline{\overline{W_{p,z+}}} = \frac{1}{r_+}\frac{d}{dr_+}\left[r_+(D_{B+}+D_{t+})\frac{d\bar{\psi}}{dr_+}\right] \tag{12}$$

where D_{B+} and D_{t+} are the coefficients of Brownian and turbulent diffusion non-dimensionalised with respect to ν_g. K_+ is a dimensionless parameter describing the rate of depletion of particles from the flow, such that $K_+ = 2\pi(r_{ow+}V_{ow+} - r_{iw+}V_{iw+})/\dot{m}_{p+}$ where $\dot{m}_{p+} = \dot{m}_p u_*/(\nu_g^2\bar{\rho}_{p,m})$ and $\dot{m}_p$ is the total particle mass flow rate.

Boundary conditions are required at the inner and outer walls and are prescribed in a manner similar to Young and Leeming (1997). The purely convective nature of the momentum equations can be accommodated by upwinding the spatial derivatives of the particle convective velocity at the inner and outer boundaries once these equations have been written in finite-difference form.

The wall boundary condition for $\bar{\psi}$ is more difficult to formulate because of the diffusive terms in the particle mass conservation equation. An expression was derived by Young and Leeming from a simple kinetic theory approach based on a Maxwellian distribution of particle velocity close to the wall. Adapting this result to the annular-flow situation, the dimensionless deposition velocities at each wall are written as,

$$V_{iw+} = \left[\bar{\psi}\overline{\overline{W_{p,r+}}} - (D_{B+}+D_{t+})\frac{d\bar{\psi}}{dr_+}\right]_{iw} = \bar{\psi}_{iw}\left[\frac{1}{2}\overline{\overline{W_{p,r+}}}[1+\mathrm{erf}(-M_r)] - \frac{\exp(-M_r^2)}{\sqrt{2\pi Sc\tau_{p+}}}\right]_{iw} \tag{13a}$$

$$V_{ow+} = \left[\bar{\psi}\overline{\overline{W_{p,r+}}} - (D_{B+}+D_{t+})\frac{d\bar{\psi}}{dr_+}\right]_{ow} = \bar{\psi}_{ow}\left[\frac{1}{2}\overline{\overline{W_{p,r+}}}[1+\mathrm{erf}(+M_r)] - \frac{\exp(-M_r^2)}{\sqrt{2\pi Sc\tau_{p+}}}\right]_{ow} \tag{13b}$$

where erf is the error function, and $M_r = \overline{\overline{W_{p,r+}}}\sqrt{Sc\tau_{p+}/2}$, Sc being the laminar Schmidt number. It should be noted that $\overline{\overline{W_{p,r+}}}$ is negative when particles move towards the inner wall and positive when they move towards the outer wall with the result that V_{iw+} and V_{ow+} are of opposite sign.

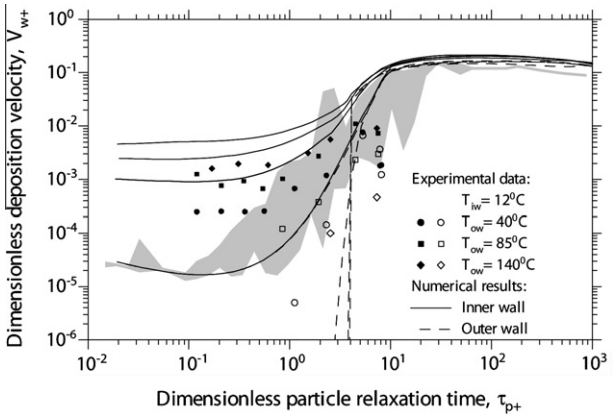

Fig. 11. Comparison between experiment and theory using the equation of Talbot et al. The lowest solid line represents the theoretical results for isothermal deposition (inner and outer walls identical). Successively higher solid lines represent inner wall deposition for successive increases in T_{ow}. Dashed lines represent outer wall deposition with T_{ow} = 85 °C and 140 °C being identical, and T_{ow} = 40 °C slightly offset.

5.2. Particle turbulence modelling

Closure of Eqs. (10) and (12) was achieved by adopting the 'local equilibrium' particle turbulence model of Young and Leeming (1997) and Slater et al. (2003) such that,

$$\overline{\overline{\left(v'_{p,r+}v'_{p,r+}\right)}} = \Gamma\overline{\left(u'_{g,r+}u'_{g,r+}\right)} \tag{14a}$$

$$\bar{\psi}\overline{\overline{u'_{g,r+}}} = -\Gamma D_{t+}\frac{\partial\bar{\psi}}{\partial r_+} \tag{14b}$$

$$D_{t+} = \nu_{gt+} \tag{14c}$$

where $u'_{g,r+} = u'_{g,r}/u_*$ and $u'_{g,r}$ is the radial component of the gas fluctuating-velocity, and $\Gamma = \tau_{g+}/(\tau_{g+}+\tau_{p+})$ where τ_{g+} is a dimensionless carrier-gas eddy time-scale given by,

$$\tau_{g+} = \frac{\nu_{gt+}}{\overline{\left(u'_{g,r+}u'_{g,r+}\right)}} \tag{15}$$

5.3. Modelling of the carrier-gas turbulence

In order to solve the particle equations a knowledge of the carrier-gas flow properties is required, specifically the radial varia-

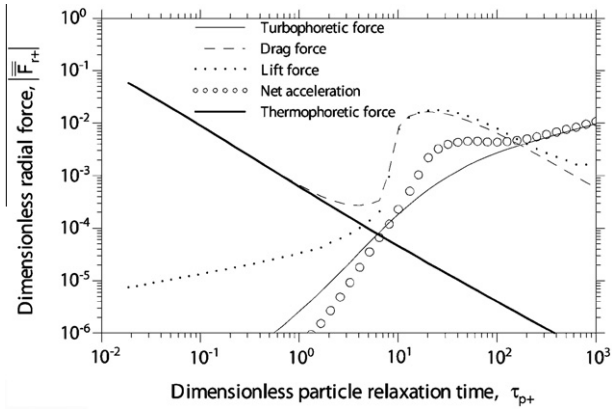

Fig. 12. Behaviour of particle radial forces at the inner wall for T_{ow} = 140 °C.

tions of $\overline{U_{g,z+}}$, $\overline{\left(u'_{g,r+}u'_{g,r+}\right)}$, v_{gt+} and the Reynolds-averaged gas temperature $\bar{T}_g$ (in order to calculate the thermophoretic force).

The carrier-gas turbulence model adopted has a strong effect on the stability of the numerical scheme. As shown by Young and Leeming (1997) and Slater et al. (2003), turbophoresis is governed by the term $-\partial\overline{\left(v'_{p,r+}v'_{p,r+}\right)}/\partial r_+$ which is a function of $\overline{\left(u'_{g,r+}u'_{g,r+}\right)}$ and v_{gt+} (through Γ). In order that the turbophoretic force has a smooth radial variation, $\overline{\left(u'_{g,r+}u'_{g,r+}\right)}$ and v_{gt+} must be twice differentiable. The best method of meeting this requirement is to use empirical expressions which fit available experimental (and/or DNS) data accurately (particularly in the near-wall region) and are also continuously differentiable. The empirical expressions used were similar to those of Young and Leeming (1997) but with alterations to account for the change in geometry from a pipe to an annulus. They are described in detail by Healy (2003) along with other aspects of the calculation of the carrier-gas flow properties.

6. A comparison of experimental and theoretical results

6.1. Theoretical calculations using the equation of Talbot et al.

As noted previously, the interpolation prescription of Talbot et al. is currently the most popular expression for the thermophoretic force on a spherical particle. Calculations using this prescription are presented in Fig. 11, together with the experimental measurements.

Fig. 11 shows that for small τ_{p+} the theoretical inner wall deposition velocity is approximately constant, its magnitude increasing with increase in outer wall temperature. In all cases, the theoretical values exceed the experimental by a factor of 3–4. The outer wall deposition velocity is initially zero because thermophoresis dominates and drives all particles from the outer wall but, as τ_{p+} increases from 1 to 10, the calculated deposition velocities at both walls increase and approach their isothermal values. The agreement of V_{ow+} with the experimental data, as it rises from a negligible level to its isothermal value, is encouraging, considering the difficulty of the measurements. The experimental points for $\tau_{p+} \geqslant 8.0$ have not been included because they are unreliable (as mentioned earlier), but it is still possible to infer from Fig. 11 that the deposition velocities of large particles are almost certainly unaltered by temperature gradients of the magnitude realised in the present series of tests.

Fig. 12 shows the variation with τ_{p+} of the magnitude of the individual radial forces at the inner wall. The thermophoretic force decreases steadily as τ_{p+} increases, while the lift and turbophoretic forces increase, the former extremely rapidly around $\tau_{p+} \approx 10$. The drag force acts to resist these forces and the convective acceleration represents the net sum of all the forces.

It is also of interest to examine the variation of certain quantities across the annulus. To this end, profiles of $\overline{\overline{W}_{p,r+}}$, $\overline{\overline{F}_{r+}}$ and $\bar{\psi}$, all plotted against y_+ (dimensionless distance from the inner wall), are presented in Fig. 13 (for isothermal flow) and Fig. 14 (for flow with thermophoresis). In these figures, it should be noted that (i) the Saffman lift force has been included in all predictions, (ii) the vertical axes for the $\bar{\psi}$ profiles have been offset from the walls for clarity, and (iii) different ordinate scales have been used for each profile. For the profiles of $\overline{\overline{W}_{p,r+}}$ and $\overline{\overline{F}_{r+}}$, a negative value represents a velocity or force towards the inner wall.

Fig. 13 shows profiles for isothermal deposition for $\tau_{p+} = 0.01$, 0.1 and 1.0. Over this range of τ_{p+} there is a steadily increasing peak of particle convective velocity in the buffer layer at $y_+ \approx 15$ resulting from the increasing dominance of turbophoresis over turbulent diffusion. This and other characteristics of Fig. 13 are discussed in the context of pipe-flow by Young and Leeming (1997) to which the reader is referred for further details.

Fig. 14 shows that the profiles are very different when thermophoresis is present. When $\tau_{p+} = 0.01$ the negative thermophoretic

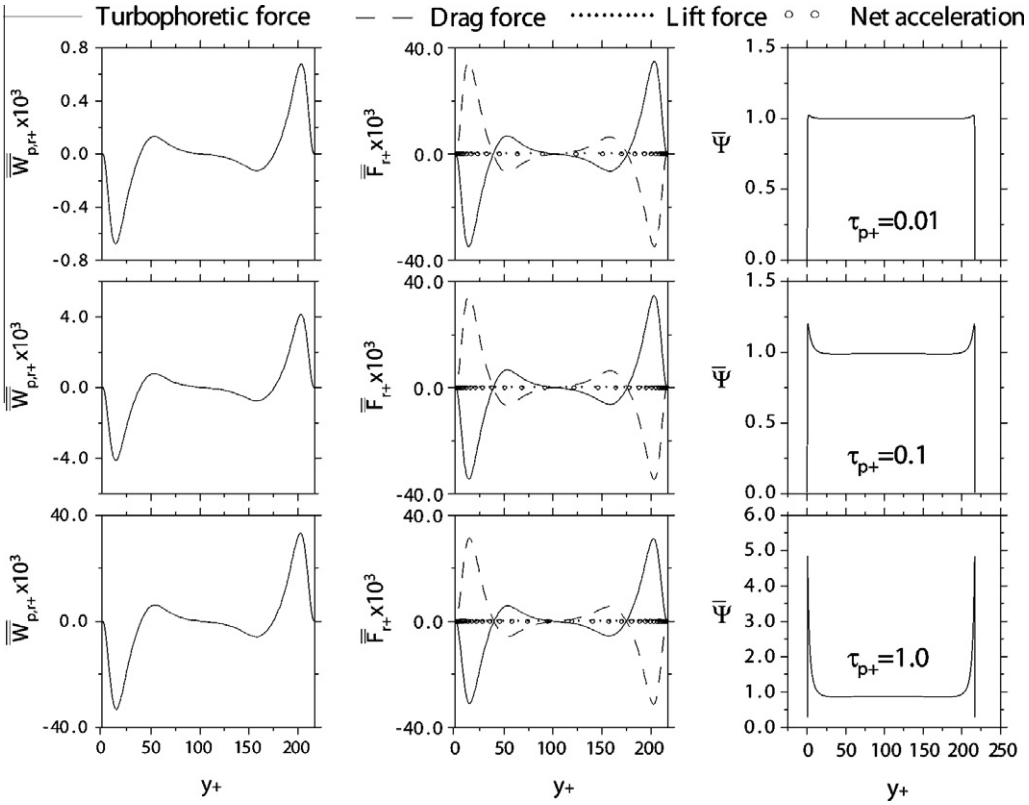

Fig. 13. Particle behaviour under isothermal conditions: dimensionless profiles of radial particle velocity, radial forces and acceleration, and particle density.

force (bold line) propels particles away from the hot outer wall (at $y_+ = 150$) and towards the cold inner wall (at $y_+ = 0$). As a result (referring to Fig. 11), V_{ow+} is negligible and V_{iw+} is significantly increased from its isothermal value. The thermophoretic force also results in a finite particle radial velocity at each wall and has the effect of reducing the near-wall peaks in particle density by directing particles at the outer wall towards the core of the flow and causing deposition of particles that were near the inner wall.

As τ_{p+} increases *Kn* decreases and the magnitude of the thermophoretic force falls. At $\tau_{p+} = 1$ the thermophoretic force is small and the other force terms are almost identical to those in the isothermal calculation of Fig. 13. Nevertheless, the small but finite thermophoretic force still has enough influence to prevent significant deposition on the hot outer wall and enhance deposition on the cold inner wall. This can be seen by the existence of a small particle radial velocity at each wall in Fig. 14. When $\tau_{p+} = 10$, however, the influence of thermophoresis (for this value of T_{ow}) is negligible.

6.2. The discrepancy between experimental and theoretical results

Fig. 11 showed that the deposition rates calculated using the expression of Talbot et al. were 3–4 times greater than those measured experimentally. The following possible sources of error were carefully examined but ultimately discarded:

(i) The thermal conductivities of uranine and oleic acid are 0.43 and 0.23 W m^{-1} K^{-1} and the thermal conductivity of a particle comprising these constituents should lie somewhere in between. Numerical calculations with the extreme values gave essentially identical results (Healy, 2003).

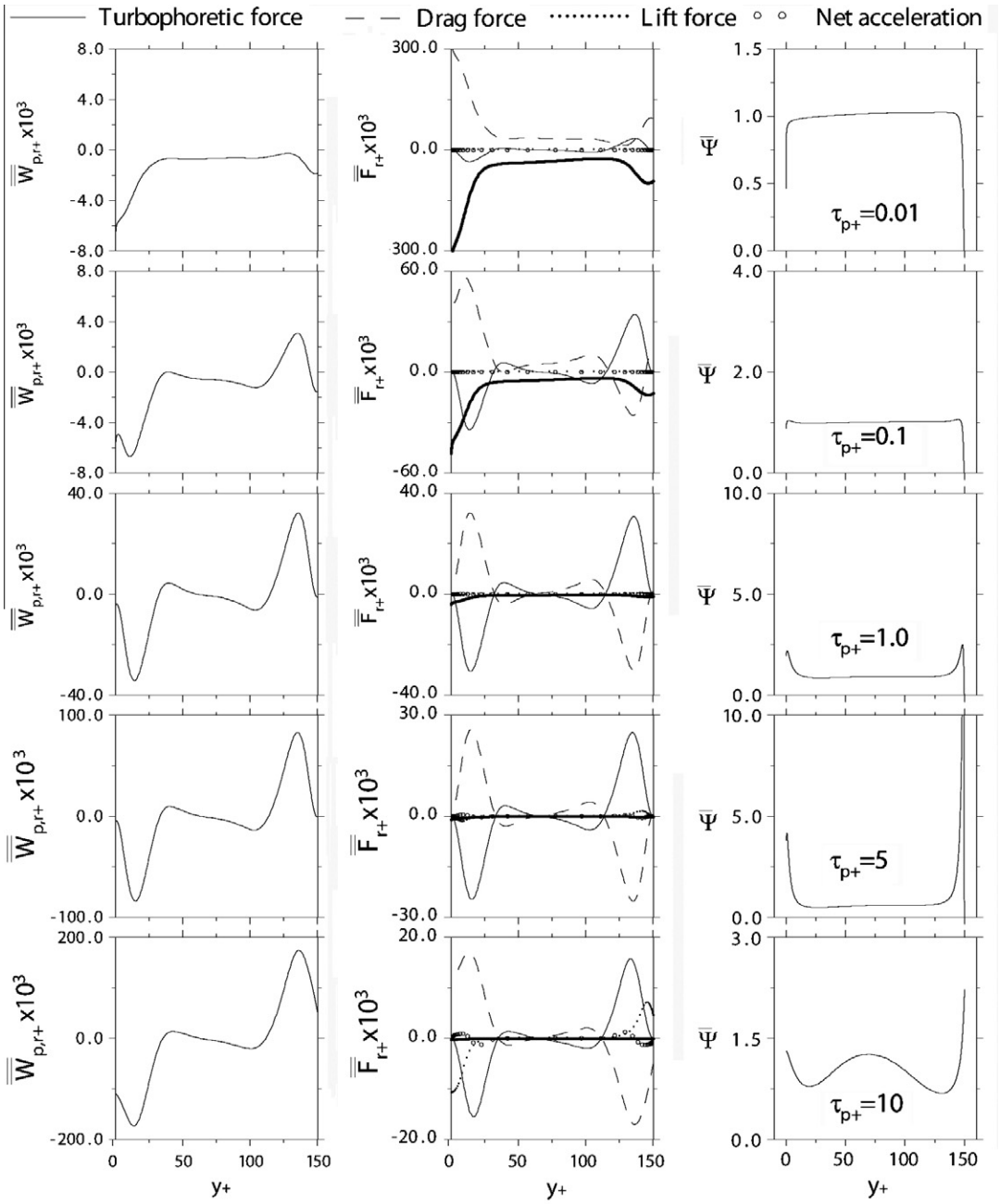

Fig. 14. Particle behaviour including thermophoresis with T_{ow} = 140 °C: dimensionless profiles of radial particle velocity, radial forces and acceleration, and particle density.

(ii) There are no experimental measurements for *non-isothermal* turbulent annular-flow but there are DNS data for plane 2D turbulent channel-flow with the walls at different temperatures (Kasagi et al., 1992). Healy (2003) used this to show that the dimensionless temperature profile used in the calculations conforms very closely to the universal profiles in the near-wall region and slight differences did not influence the deposition velocities. The closure model for the turbulent Prandtl number of the carrier-gas was also found to be unimportant.

(iii) Variations in the carrier-gas radial fluctuating-velocity and eddy viscosity profiles were examined. Changes in eddy viscosity had little effect but, in the region where thermophoresis and turbophoresis are of comparable importance, the deposition velocity V_{iw+} was sensitive to variations in the fluctuating-velocity distribution in the buffer layer. However, for smaller values of τ_{p+} where turbophoresis is unimportant, V_{iw+} was unaffected.

(iv) The thermophoretic force was based solely on the mean temperature gradient. The neglect of temperature fluctuations is difficult to justify but the DNS study of thermophoretic deposition by Thakurta et al. (1998) found that the inclusion of temperature fluctuations had virtually no effect on the results and the same conclusion was reached by Kroger and Drossinos (2000) in their random walk calculations.

(v) The sensitivity to errors in the wall temperatures was investigated by performing calculations where the inner wall temperature was increased by 5 °C and the outer wall temperature was reduced by 5 °C. This would represent a fairly large measuring error. As discussed by Healy (2003), the agreement between theory and experiment was improved but a much greater variation would be required to achieve a satisfactory match. An error of this magnitude is considered unlikely.

From the above it appears that there is a definite discrepancy between the experimental deposition velocities and the predictions using the equation of Talbot et al. In Section 2, doubts were expressed about the accuracy of this curve fit and the more theoretically based equation of Beresnev and Chernyak will now be examined.

Fig. 15 shows values of $-\Phi/(2\pi)$ plotted against $\log_{10}(Kn)$ for uranine and oleic acid ($\Lambda \cong 16$) as used in the present study. The three curves represent the interpolating prescription of Talbot et al. (1980), the theory of Beresnev and Chernyak (1995) and the theory of Yamamoto and Ishihara (1988), the latter included

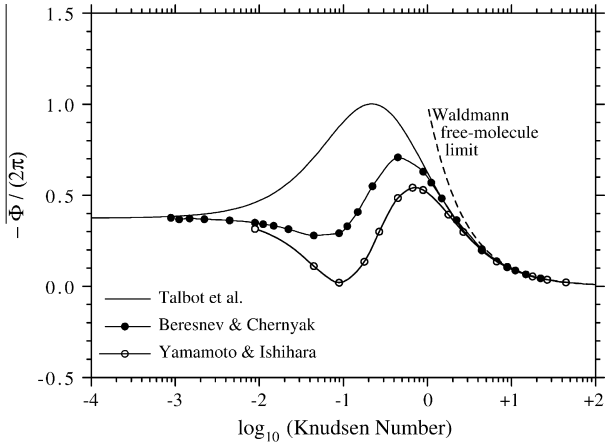

Fig. 15. Theoretical curves of $-\Phi/(2\pi)$ plotted against $\log_{10}(Kn)$ for uranine and oleic acid particles, $\Lambda \cong 16$ and $\alpha_m = \alpha_e = 1$.

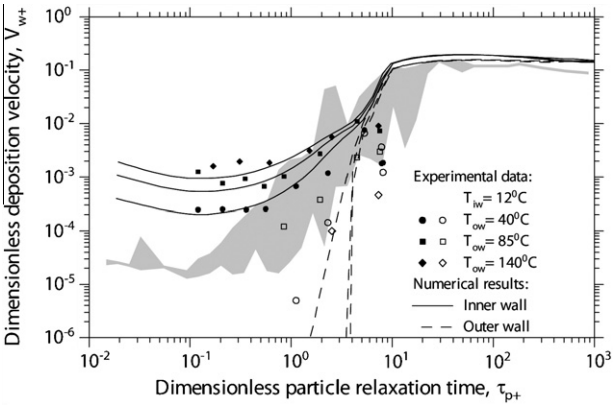

Fig. 16. Comparison between experiment and calculation using the full theory of Beresnev and Chernyak. Successively higher solid lines represent inner wall deposition for successive increases in T_{ow}. Dashed lines represent outer wall deposition with T_{ow} = 85 °C and 140 °C being coincident and T_{ow} = 40 °C slightly offset.

for interest only. There are clearly considerable discrepancies between the three curves. In the range where thermophoresis has the greatest effect on deposition ($0.1 < \tau_{p+} < 1$), the values of Kn lie between 0.01 and 0.1. Fig. 15 suggests that the use of the Beresnev and Chernyak theory should result in reduced deposition velocities in this range.

Fig. 16 shows the results of calculations using the Beresnev and Chernyak theory. The agreement with the experimental data is greatly improved; indeed, it is now extremely good. It should be noted that V_{iw+} first decreases with increasing τ_{p+} in contrast to the results of Fig. 11 using the Talbot et al. expression where V_{iw+} remains almost constant. Also of interest is the subsequent increase in deposition velocity resulting from the increasing dominance of turbophoresis which appears to start at around $\tau_{p+} \cong 0.1$.

7. Conclusions

A new set of experimental measurements for particle deposition in a turbulent annular-flow with different cross-stream temperature gradients has been obtained. The success of the experiments was made possible by the use of an annular-flow geometry which allowed an approximately constant temperature difference between the inner and outer walls to be established over a large axial distance. A numerical study has also been undertaken and it has been found that the widely-used expression of Talbot et al. (1980) does not give the correct thermophoretic force for the thermal conductivity ratio and range of Knudsen numbers used. The theory of Beresnev and Chernyak (1995) gives much better results because it takes account of the second mechanism of thermophoresis. This makes it applicable to a broader range of conditions. The experimental and theoretical studies revealed the existence of a regime where thermophoresis and turbophoresis are of comparable importance for deposition and reinforce each other. The experimental results should provide reliable data for future studies of thermophoresis and particle deposition in more complex flow geometries.

Acknowledgements

The work was funded by the then PowerGen Power Technology Centre, Ratcliffe-on-Soar. The authors wish to thank Dr. A.D. Leeming who developed the original particle pipe-flow code and Mr. Roy Slater who constructed the experimental equipment. They are also grateful to Dr. J.E. Fackrell formerly of PowerGen for his

support and technical advice. DPH was supported by a Cambridge University Domestic Research Studentship with maintenance contributions from PowerGen, the Ford of Britain Trust and the Rex Moir Fund of the Cambridge University Engineering Department.

References

Al-Azzawi, H.K., Owen, I., 1984. Measuring the thermal conductivity of uranine. Int. J. Heat Fluid Flow 5, 57–59.
Bakanov, S.P., 1991. Thermophoresis in gases at small Knudsen numbers. Aerosol Sci. Technol. 15, 77–92.
Beresnev, S., Chernyak, V., 1995. Thermophoresis of a spherical particle in a rarefied gas: numerical analysis based on the model kinetic equations. Phys. Fluids 7, 1743–1756.
Brock, J.R., 1962. On the theory of thermal forces acting on aerosol particles. J. Colloid Sci. 17, 768–780.
Chung, S.Y., Rhee, G.H., Sung, H.J., 2002. Direct numerical simulation of turbulent concentric annular pipe flow – Part 1: Flow field. Int. J. Heat Fluid Flow 23, 426–440.
Dwyer, H.A., 1967. Thirteen-moment theory of the thermal force on a spherical particle. Phys. Fluids 10, 976–984.
Epstein, P.S., 1929. Zur Theorie des Radiometers. Z. Physik 54, 537–563.
Healy, D.P., 2003. On the Full Lagrangian Approach and Thermophoretic Deposition in Gas-particle Flows. Ph.D. thesis. Cambridge University Engineering Department.
Jacobsen, S., Brock, J.R., 1965. The thermal force on spherical sodium chloride aerosols. J. Colloid Sci. 20, 544–554.
Kasagi, N., Tomita, Y., Kuroda, A., 1992. Direct numerical simulation of passive scalar field in a turbulent channel flow. ASME J. Heat Transfer 114, 598–606.
Kroger, C., Drossinos, Y., 2000. A random-walk simulation of thermophoretic particle deposition in a turbulent boundary layer. Int. J. Multiphase Flow 26, 1325–1350.
Leeming, A.D., 1995. Particle Deposition from Turbulent Flows. Ph.D. thesis. Cambridge University Engineering Department.
Li, W., Davis, E.J., 1995a. Measurement of the thermophoretic force by electrodynamic levitation: microspheres in air. J. Aerosol Sci. 26, 1063–1083.
Li, W., Davis, E.J., 1995b. The effects of gas and particle properties on thermophoresis. J. Aerosol Sci. 26, 1085–1099.
Liu, B.Y.H., Agarwal, J.K., 1974. Experimental observation of aerosol deposition in turbulent flow. J. Aerosol Sci. 5, 145–155.
Montassier, N., Boulaud, D., Renoux, A., 1991. Experimental study of thermophoretic particle deposition in laminar tube flow. J. Aerosol Sci. 22, 677–687.
Romay, F.J., Takagaki, S.S., Pui, D.Y.H., Liu, B.Y.H., 1998. Thermophoretic deposition of aerosol particles in turbulent pipe flow. J. Aerosol Sci. 29, 943–959.
Schmitt, K.H., 1959. Untersuchungen an Schwebstoffteilchen im Temperaturfeld. Z. Naturforschung 14a, 870–881.
Sehmel, G.A., 1968. Aerosol Deposition from Turbulent Airstreams in Vertical Conduits. R&D Report BNWL-578. US Atomic Energy Commission, Batelle Northwest Laboratory.
Shakhov, E.M., 1968. Generalisation of the Krook kinetic relaxation equation. Fluid Dyn. 3 (5), 95–96.
Slater, S.A., Leeming, A.D., Young, J.B., 2003. Particle deposition from two-dimensional turbulent gas flows. Int. J. Multiphase Flow 29, 721–750.
Sone, Y., 1972. Flow induced by thermal stress in rarefied gas. Phys. Fluids 15, 1418–1423.
Talbot, L., Cheng, R.K., Schefer, R.W., Willis, D.R., 1980. Thermophoresis of particles in a heated boundary layer. J. Fluid Mech. 80, 737–758.
Thakurta, D.G., Chen, M., McLaughlin, J.B., Kontomaris, K., 1998. Thermophoretic deposition of small particles in a direct numerical simulation of turbulent channel flow. Int. J. Heat Mass Transfer 41, 4167–4182.
Waldmann, L., 1959. Uber die Kraft eines inhomogen Gases auf kleine suspendierte Kugeln. Z. Naturforschung A14, 589–599.
Wells, A.C., Chamberlain, A.C., 1967. Transport of small particles to vertical surfaces. Brit. J. Appl. Phys. 18, 1793–1799.
Yamamoto, K., Ishihara, Y., 1988. Thermophoresis of a spherical particle in a rarefied gas of a transition regime. Phys. Fluids 31, 3618–3624.
Young, J.B., Leeming, A.D., 1997. A theory of particle deposition in turbulent pipe flow. J. Fluid Mech. 340, 129–159.